Acta of Bioengineering and Biomechanics
Vol. 27, No. 4, 2025

Original paper
DOI: 10.37190/abb/218065

Stress distribution in endocrowns with different materials and loading conditions: a FEM study

DRAGOSLAV LAZIC[1], MILAN BOJOVIC[1]*, MILAN BLAGOJEVIC[2],
JELENA VULOVIC[3], SANJA JOVANOVIC[1]

[1] University of Priština, Faculty of Medicine, Department of Dentistry, Serbia.
[2] University of Priština, Faculty of Technical Sciences, Serbia.
[3] University of Belgrade, Faculty of Dental Medicine, Serbia.

Purpose: This study aimed to evaluate the effect of different restorative materials on stress distribution in endodontically treated teeth restored with endocrowns using the finite element analysis (FEA). *Methods*: Six test groups were defined according to restorative material: (1) polyetheretherketone (PEEK) with composite veneer, (2) carbon fiber-reinforced PEEK (CFR-PEEK) with composite veneer, (3) glass fiber-reinforced PEEK (GFR-PEEK) with composite veneer, (4) cobalt–chromium (Co-Cr) alloy with ceramic veneer, (5) monolithic lithium disilicate (LiDi) and (6) monolithic zirconium dioxide (Y-TZP). Mandibular molar models were designed in SolidWorks 2018 and Meshmixer and analyzed using ANSYS 16.0 under occlusal (400–600 N) and lateral (200–400 N) loading. Stress distribution in dentin was assessed using the von Mises criterion. *Results*: LiDi demonstrated a uniform and diffuse stress distribution with minimal peak variations, favoring its use under lateral loading. GFR-PEEK significantly reduced the dentin volume exposed to critical stress thresholds under high occlusal forces. In contrast, Co-Cr alloy and Y-TZP exhibited greater stiffness, resulting in less favorable stress transfer and pronounced concentration zones compared with PEEK-based materials and LiDi. *Conclusions*: The restorative material has a decisive influence on the biomechanical behavior of endocrowns. LiDi appears more suitable for premolars predominantly subjected to lateral forces, while GFR-PEEK offers superior protection in molars exposed to heavy occlusal loading.

Key words: *endocrowns, finite element analysis, stress distribution, restorative materials, endodontically treated teeth*

1. Introduction

Prosthetic rehabilitation of endodontically treated teeth with extensive loss of coronal structure remains a major challenge in contemporary dentistry. Successful management requires the use of advanced restorative materials. The reduced fracture resistance of these teeth is considered to be primarily associated with the loss of dental tissue caused by trauma or carious destruction, and to a lesser extent with dehydration and structural alterations of dentin [13], [20]. The integration of computer-aided design/computer-aided manufacturing (CAD/CAM) technology and adhesive systems into clinical practice has established endocrowns as a reliable approach for restoring endodontically treated teeth [7]. Endocrowns are single-unit restorations, or two-part restorations when a primary framework is present, designed specifically for the restoration of endodontically treated teeth [29].

Minimally invasive tooth preparation with maximal preservation of sound structure is a fundamental principle of restorative dentistry, and the use of endocrowns strongly supports this concept. When present, a circumferential ferrule of at least 1 mm may enhance fracture resistance, although endocrowns primarily rely on pulp chamber retention [9]. Through adhesive cementation, the restoration and tooth form an integrated unit [12]. Long-term success depends on minimizing stress on the remaining tissues, achieved by an appropriate prepa-

* Corresponding author: Milan Bojović, University of Priština, Faculty of Medicine, Department of Dentistry, Serbia, e-mail: milan_dent@hotmail.com
Received: October 29th, 2025
Accepted for publication: February 11th, 2026

ration design and the selection of restorative materials that provide optimal function with minimal biological cost [4]. Endocrowns are increasingly indicated in cases with reduced interocclusal space, short, curved or calcified roots [24]. The mechanical properties of restorative materials play a decisive role in the biomechanical behavior of the tooth-restoration complex and in the longevity of the prosthesis. Elastic modulus is particularly important, because closer matching between the tooth and the restorative material helps preserve dentin integrity under both functional and parafunctional loading. [19].

In modern restorative dentistry, endocrowns can be fabricated from a variety of materials, including high-performance polymers such as PEEK and its fiber-reinforced derivatives (CFR-PEEK, GFR-PEEK), base metal alloys (e.g., Co-Cr), and advanced ceramics such as LiDi and Y-TZP. The mechanical and esthetic characteristics of each material largely determine their clinical application [10]. LiDi is well established for endocrown use, combining favorable strength, adhesive bonding potential, and translucency, with encouraging clinical outcomes reported after 2–3 years of follow-up [7]. Y-TZP, on the other hand, provides superior fracture resistance and toughness, but its adhesive cementation is technically challenging since, unlike glass-containing ceramics, it cannot be hydrofluoric-acid etched, requiring alternative conditioning and bonding methods [3]. Co-Cr alloys exhibit high mechanical durability, excellent wear and corrosion resistance, but present obvious esthetic limitations [33]. PEEK demonstrates a relatively low elastic modulus (~3–4 GPa), closer to dentin than metals and Y-TZP, which may contribute to more favorable stress distribution; fiber reinforcement with carbon or glass improves stiffness and strength, although adhesion and esthetics remain limitations [26]. Few investigations to date have concurrently assessed axial and lateral loading across these material groups, under different load magnitudes and standardized boundary conditions, while applying multiple descriptive criteria within finite element analysis. This comprehensive approach is the focus of the present study.

Finite element analysis (FEA) provides valuable insights into stress distribution, guiding both restoration design and material selection [31]. The question of the optimal elastic modulus for materials used in the restoration of such teeth, however, remains without a definitive answer.

The working hypothesis of this study was that the restorative material, in correlation with the direction and intensity of loading, significantly affects stress distribution in the remaining tooth structure of endodontically treated teeth restored with endocrowns. We assumed that materials with an elastic modulus closer to dentin, such as PEEK, GFR-PEEK, and CFR-PEEK, would provide more favorable stress distribution and reduce the risk of localized concentrations, whereas stiffer materials with higher modulus values, such as Co-Cr alloy and Y-TZP, would result in more pronounced stress peaks.

2. Materials and methods

Geometric modeling

The finite element analysis was developed from the geometry of a real human tooth extracted for periodontal reasons. Specifically, a left mandibular first permanent molar (M1) was obtained from the tooth bank of the University of Priština, Faculty of Medicine, Department of Dentistry.

The external tooth geometry was acquired by optical scanning using an intraoral scanner (Shining 3D Aoralscan, Shining 3D Tech. Co., China), producing a triangulated surface (STL) model. The STL file was subsequently processed in CAD software to perform surface smoothing, geometric correction, and reconstruction of anatomically consistent smooth surfaces. Within the same CAD workflow, the internal tooth morphology, including the pulp chamber, was reconstructed and the endocrown restoration geometry was designed. The finalized geometric model was then exported in STEP format and used for further CAD refinement and finite element analysis.

The triangulated surface file (STL) was imported into SolidWorks 2018 (Dassault Systèmes SolidWorks Corp., Waltham, MA, USA), where reverse engineering was applied to reconstruct smooth NURBS surfaces of the coronal and radicular segments. The pulp chamber was generated in Meshmixer (Autodesk, Inc., San Rafael, CA, USA) using the Hollow function to create a uniform wall thickness of approximately 3.0 mm. The tooth was segmented at the cemento-enamel junction (CEJ) into coronal and radicular components. A circumferential ferrule (1.0 mm in height and thickness) was modeled on the radicular segment (11 × 18 × 12 mm). The periodontal ligament (PDL) was modeled as a circumferential layer (0.20–0.25 mm) using the Offset function in Meshmixer. Gutta-percha was generated within the modeling environment and positioned in the root canals (10.42 mm mesiobuccal, 11.2 mm distal). The bone model was reconstructed from cone-beam computed tomography (CBCT) imaging of the mandibular first molar region. A representative cross-section was extruded in Fusion 360 (Autodesk, Inc.) to produce a 3D segment (10 mm mesiodistal length) composed of a trabecular core (10 mm buccolingual × 19 mm height) surrounded by a 1.5 mm cortical shell (Fig. 1).

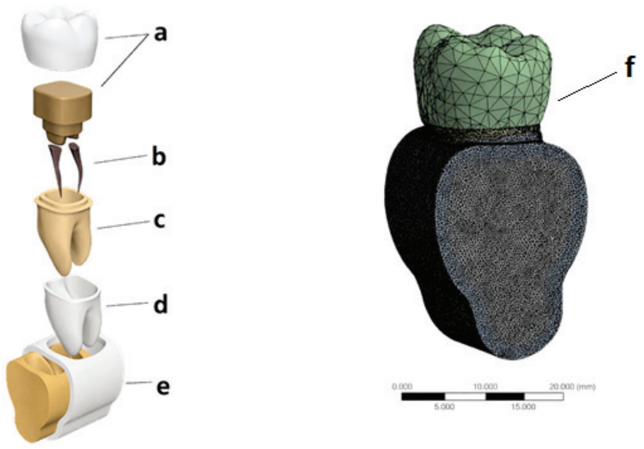

Fig. 1. 3D finite element model of mandibular molar: (a) endocrown configuration (framework, veneer, and monolithic crown), (b) root canal filling, (c) root, (d) periodontal ligament, (e) alveolar bone segment, (f) FEM model

Endocrown configurations

The endocrown was modeled as a bilayer restoration consisting of a primary framework (10.8 × 10.3 × 10.7 mm) and a coronal portion 5.3 mm in height, veneered with different materials depending on the experimental group, with an average veneer thickness of 1.5 mm to reproduce the final anatomical morphology. The primary framework was adapted to the geometry of the pulp chamber (4 mm in height) and included retentive extensions projecting 2 mm into the root canal space, providing macromechanical retention (Fig. 1). Six endocrown configurations were analyzed: 1) PEEK framework veneered with CAD/CAM resin composite, 2) CFR-PEEK framework veneered with CAD/CAM resin composite, 3) GFR-PEEK framework veneered with CAD/CAM resin composite, 4) Co-Cr alloy framework veneered with ceramic, 5. LiDi, and 6. Y-TZP. All materials were assumed to be homogeneous, isotropic and linearly elastic.

Material properties

Material properties, specifically Young's modulus and Poisson's ratio, were adopted from literature summarized in Table 1.

Boundary conditions and applied loads

A linear static structural analysis was performed in ANSYS 16.0 (ANSYS, Canonsburg, PA, USA). All simulations were solved under the assumption of linear-elastic material behaviour and small deformations. Occlusal (vertical) loads of 400, 500 and 600 N were applied at the distal segment of the central fissure as a uniformly distributed load over 20 mm^2, whereas lateral loads of 200, 300 and 400 N were applied to the middle third of the buccal slope of the mesiobuccal cusp as a uniformly distributed load over 6 mm^2. Occlusal loading was introduced as a distributed load over the selected occlusal contact area(s) (Figs. 2–4), representing clinically relevant antagonist contact regions. This approach avoids stress singularities typical for point loading and provides a stable and physically meaningful representation of force transfer into the restoration–tooth complex. The same loading areas and load magnitudes/directions were used in all simulations to ensure consistent comparative assessment across restorative materials and loading conditions [25], [27], [30].

Table 1. Mechanical properties of the materials used in the finite element analysis

Material	Young's modulus [MPa]	Poisson's ratio ν	Reference
Dentin	18600	0.32	[36]
Periodontal ligament	68.9	0.45	[17]
Cortical bone	10700	0.30	[2]
Spongious bone	1370	0.30	[17]
Gutta-percha	0.69	0.45	[18]
CAD/CAM resin composite	16300	0.45	[36]
PEEK	5100	0.30	[21]
GFR-PEEK	12000	0.40	[28]
CFR-PEEK	18000	0.39	[28]
Co-Cr alloy	23500	0.33	[5]
LiDi	95000	0.25	[37]
Y-TZP	210000	0.30	[38]

All contact interfaces between model components were defined as bonded, assuming perfect adhesion without sliding or separation. The finite-element discretization consisted of 249 889 nodes and 1 158 875 tetrahedral elements, providing sufficient mesh density for numerical stability and convergence of the stress field in the region of interest.

The outcomes of interest were stresses within the restored tooth (endocrown–cement–dentin–enamel complex), while stresses and displacements in the mandibular bone were not considered. Therefore, the mandibular segment was treated primarily as a structural support and the model was truncated. To prevent rigid body motion and ensure numerical stability, a fixed support condition was introduced on the bone support region, constraining all translational degrees of freedom ($U_x = U_y = U_z$

= 0) (Fig. 2), consistent with established finite element workflows in dental biomechanics [14], [34]. In accordance with the study scope, the interpretation is restricted to the tooth/restoration region, away from the artificial boundaries, since boundary conditions were kept identical across all cases, the observed differences in stress distribution can be attributed primarily to restorative material properties and loading configuration rather than to variability in support conditions [27].

Axial (occlusal) loading was applied as a uniformly distributed vertical force over the predefined occlusal contact area, simulating physiological masticatory forces transmitted through cusp–fossa contacts (Fig. 3). Lateral loading was applied as a uniformly distributed horizontal force to the buccal incline of the mesiobuccal

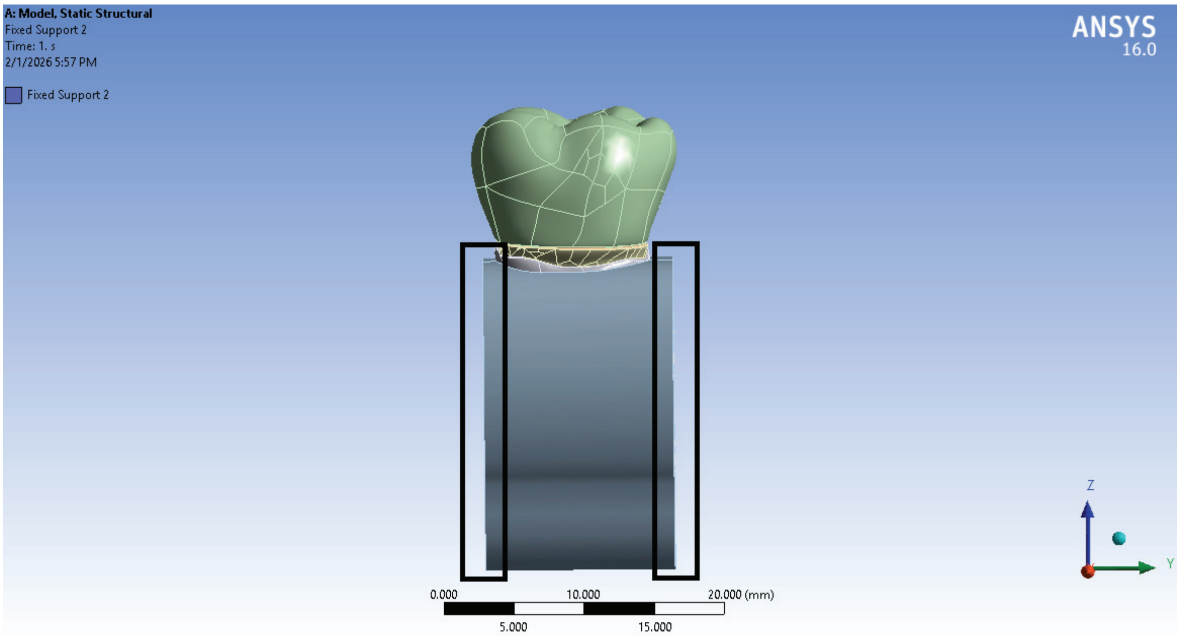

Fig. 2. Finite element model showing the location of the fixed support applied to the lateral side, medial and distal, of the alveolar bone segment

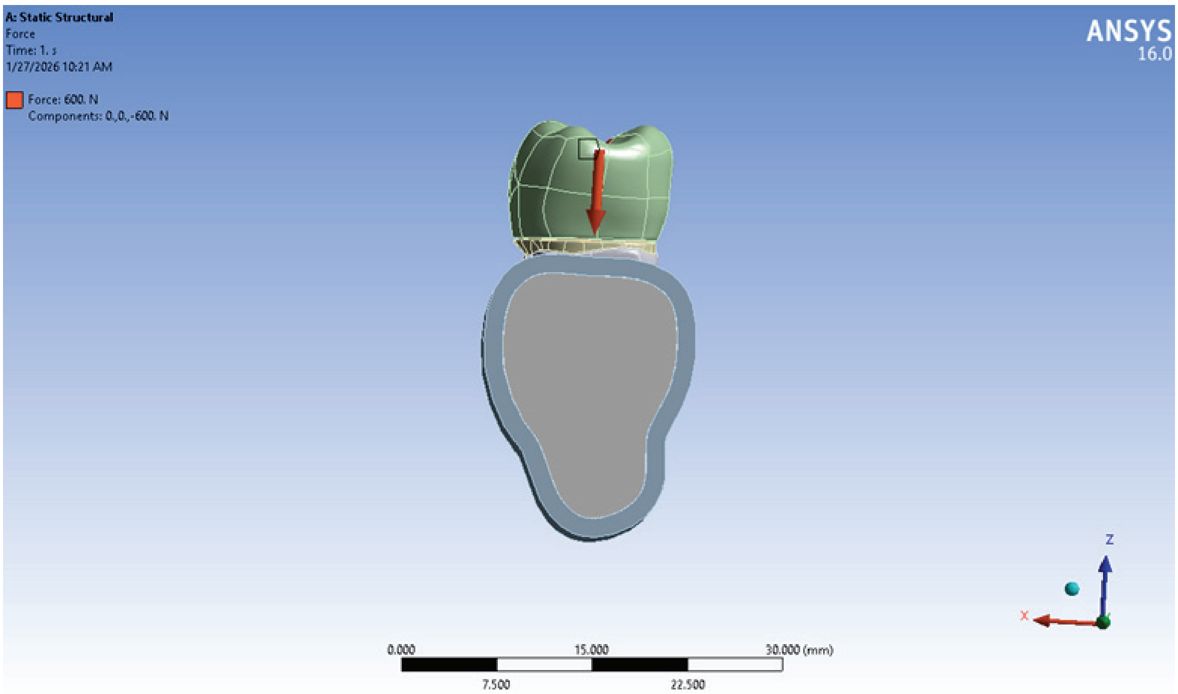

Fig. 3. Finite element model illustrates axial (occlusal) loading. A uniformly distributed vertical load was applied to the occlusal contact area to simulate physiological masticatory forces

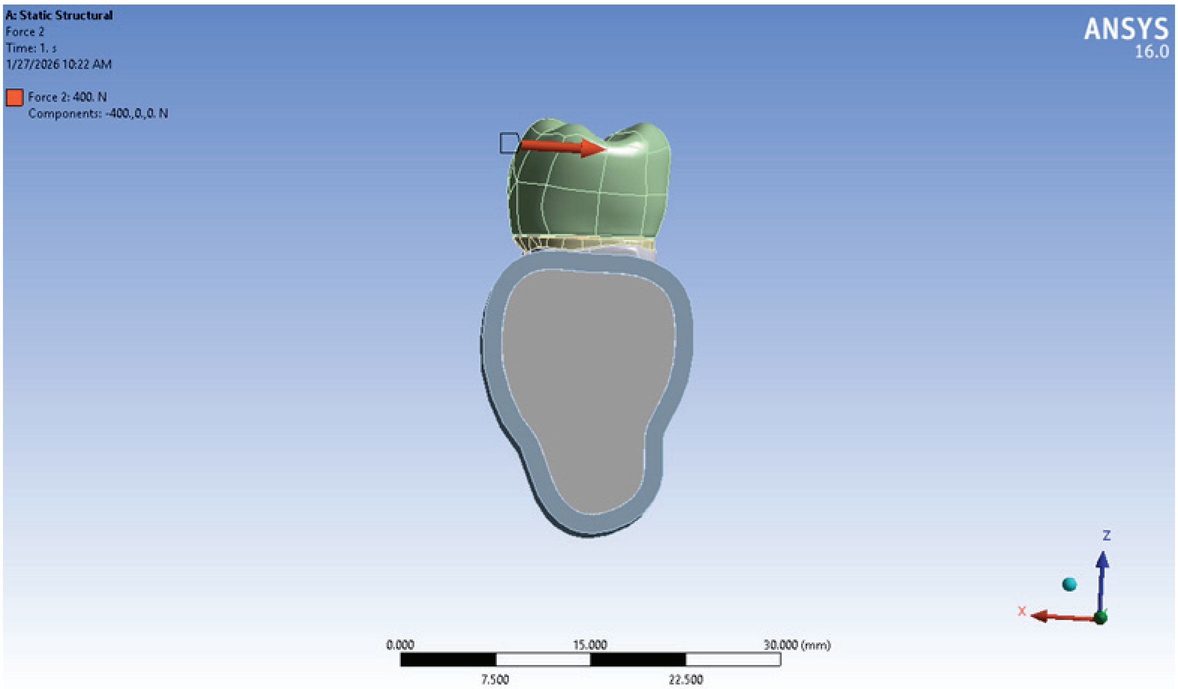

Fig. 4. Finite element model illustrating lateral loading. A uniformly distributed horizontal force was applied to the buccal incline of the mesiobuccal cusp to simulate non-axial functional or parafunctional conditions

cusp to reproduce non-axial functional or parafunctional loading conditions encountered during mastication and lateral excursions (Fig. 4).

Analytical stress indicators

In this study, stress distribution within the remaining dentin was characterized using a set of descriptive measures designed to minimize the influence of numerical artifacts and mesh dependency, thereby ensuring comparability across materials and loading conditions. The metric set included: (i) the 95th percentile stress ($p95$), (ii) the tail gap, and (iii) the high-stress fraction ($f \geq T$). All measures were derived from the empirical cumulative distribution function (ECDF) of nodal von Mises stresses, and, when available, also in their volumetric form by incorporating elemental volumes (EVOL). The 95th percentile stress (σ_{p95}) represents the stress value below which 95% of points in the dentin region are located; it provides a robust summary of the upper tail of the distribution and is less sensitive to single extreme values than the absolute maximum.

$$\sigma_{p95} = \text{percentil}_{95}(\sigma_i).$$

The tail gap was defined as the difference between the absolute maximum stress and the 95th percentile ($\sigma_{max} - \sigma_{p95}$). This measure reflects the sharpness of local stress concentrations: smaller tail gap values indicate smoother stress gradients and more uniform stress dispersion, whereas larger values denote pronounced, localized hot spots.

$$\text{tail gap} = \sigma_{max} - \sigma_{p95}.$$

The high-stress fraction ($f \geq T$) was defined as the proportion of points with $\sigma \geq T$, where the baseline threshold was set at 60 MPa, with sensitivity analyses additionally performed at 80 and 100 MPa. Lower $f \geq T$ values indicate that a smaller portion of the domain is subjected to potentially critical stress levels. When element volume data (EVOL) were available, both nodal and volumetric fractions were calculated, the latter obtained as the ratio of the summed volumes of elements exceeding the threshold to the total model volume.

$$f \geq T^{\text{nodal}} = \frac{N(\sigma_i \geq T)}{N_{\text{total}}},$$

$$f \geq T^{\text{vol}} = \frac{\Sigma V_j(\sigma_j \geq T)}{\Sigma V_j}.$$

The $p95$ and tail gap values were derived from the empirical cumulative distribution function (ECDF), where $p95$ corresponds to the 95th percentile and the tail gap is calculated as the difference between σ_{max} and σ_{p95}. The high-stress fraction ($f \geq T$) was computed as the ratio of the number of nodes (or element volumes) with stress above the defined threshold to the total number of nodes (or total volume). Lower values of all three indicators were interpreted as reflecting a more favorable and uniform stress distribution, with a reduced likelihood of sharply localized high-stress regions.

Stress distribution analysis

Stress maps were generated for each loading scenario and assessed with emphasis on the remaining dentin. Analyses were performed across all six endocrown configurations, as previously described in the Endocrown Configurations section (Figs. 5, 6).

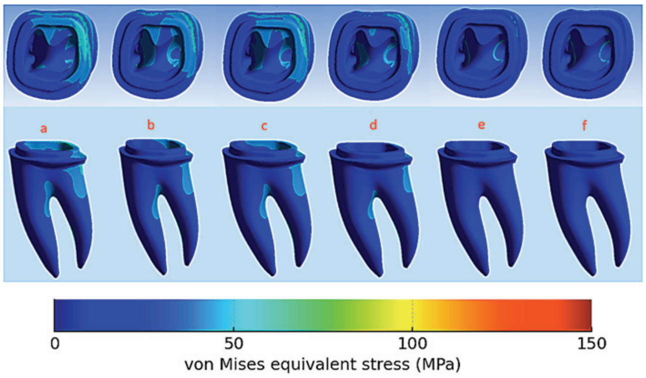

Fig. 5. Representative von Mises stress distribution in dentin for the six restorative material groups under occlusal loading: (a) PEEK, (b) CFR-PEEK, (c) GFR-PEEK, (d) Co-Cr alloy, (e) LiDi and (f) Y-TZP. Stress concentrations are indicated according to the color scale (0–150 MPa)

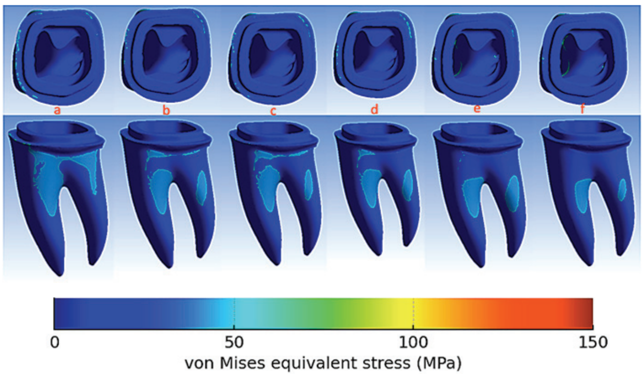

Fig. 6. Representative von Mises stress distribution in dentin for the six restorative material groups under lateral loading: (a) PEEK, (b) CFR-PEEK, (c) GFR-PEEK, (d) Co-Cr alloy, (e) LiDi and (f) Y-TZP. Stress concentrations are indicated according to the color scale (0–150 MPa)

3. Results

Under lateral loading conditions (200–400 N), all restorative materials exhibited an increase in σ_{p95} values with load intensity. PEEK and GFR-PEEK showed the lowest stress percentiles, indicating more favorable stress dissipation within dentin. LiDi and CFR-PEEK demonstrated intermediate values, while Co-Cr alloy and Y-TZP consistently produced the highest σ_{p95} levels, reflecting greater stress concentration (Fig. 7).

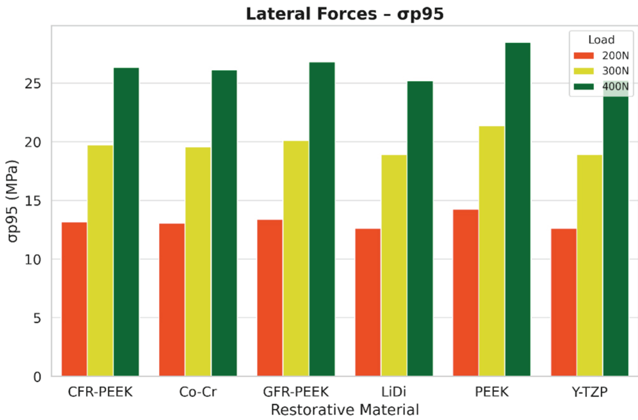

Fig. 7. Comparison of the 95th percentile stress (σ_{p95}) values in dentin under lateral loading (200–400 N) for different restorative materials. Lower σ_{p95} values indicate more uniform stress distribution, whereas higher values reflect localized stress concentrations

Tail gap analysis under lateral loading (200–400 N) demonstrated that PEEK and GFR-PEEK generated the lowest values, indicating smoother stress gradients within dentin. In contrast, Co-Cr and Y-TZP exhibited the highest tail gap values, reflecting localized stress concentrations (Fig. 8).

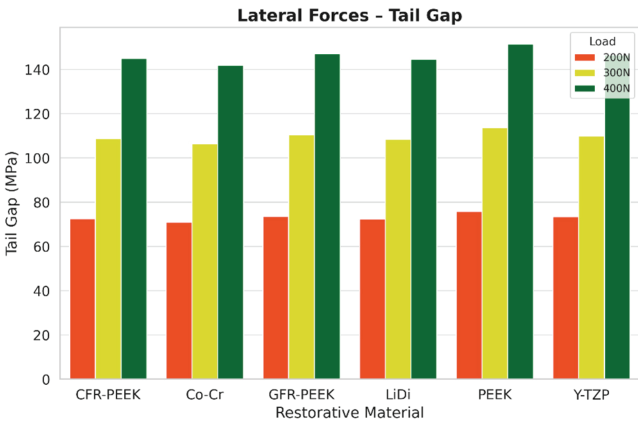

Fig. 8. Tail gap values ($\sigma_{max} - \sigma_{p95}$) in dentin under lateral loading (200–400 N) for different restorative materials. Lower tail gap values indicate smoother stress transitions, while higher values reflect the presence of localized stress concentrations

The high-stress fraction ($f \geq 60$) under lateral loading confirmed these findings. PEEK and GFR-PEEK subjected only a minimal portion of dentin to critical stress levels, while Co-Cr and Y-TZP exposed a larger dentin volume to stresses above 60 MPa (Fig. 9).

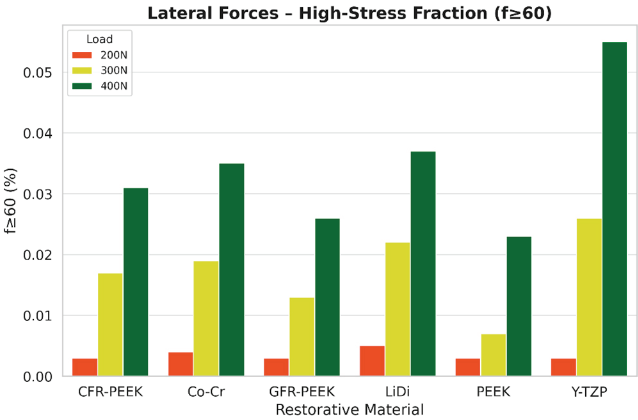

Fig. 9. High-stress fraction ($f \geq 60$) in dentin under lateral loading (200–400 N). A lower fraction denotes reduced dentin volume exposed to critical stress, whereas higher fractions suggest more extensive dentin involvement above the 60 MPa threshold

Under occlusal loading conditions (400–600 N), PEEK and GFR-PEEK consistently exhibited the lowest σ_{p95} values, suggesting more uniform stress distribution in dentin. CFR-PEEK and LiDi showed intermediate stress levels, whereas Co-Cr alloy and Y-TZP produced the highest σ_{p95} values, indicating more pronounced stress concentration (Fig. 10).

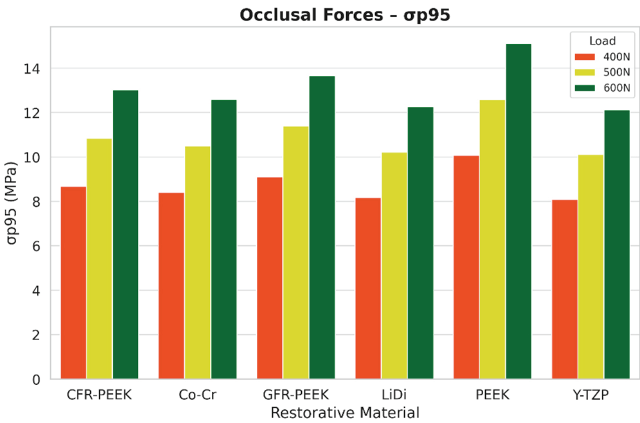

Fig. 10. Comparison of the 95th percentile stress (σ_{p95}) values in dentin under occlusal loading (400–600 N) for different restorative materials. Lower σ_{p95} values represent favorable stress dissipation, while higher values indicate localized stress accumulation

Tail gap analysis under occlusal loading revealed that PEEK-based restorations produced the smallest differences between maximum and 95th percentile stresses, indicating smoother stress gradients. In contrast, Co-Cr and Y-TZP exhibited the highest tail gap values, reflecting the presence of localized stress peaks (Fig. 11).

The high-stress fraction ($f \geq 60$) confirmed these findings: PEEK and GFR-PEEK exposed only a minimal portion of dentin to critical stress levels, while Co-Cr and Y-TZP subjected a considerably larger fraction of dentin to stresses above 60 MPa (Fig. 12).

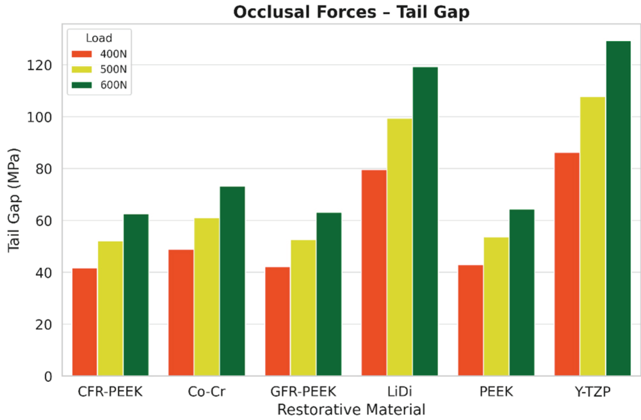

Fig. 11. Tail gap values ($\sigma_{max} - \sigma_{p95}$) in dentin under occlusal loading (400–600 N) for different restorative materials. Lower tail gap values represent smoother stress gradients and more uniform stress distribution, while higher values indicate localized stress peaks

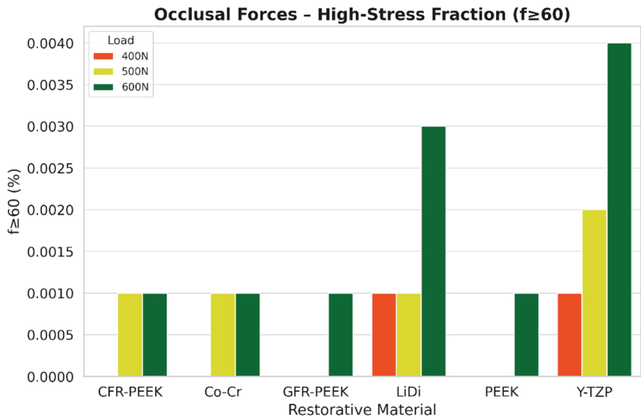

Fig. 12. High-stress fraction ($f \geq 60$) in dentin under occlusal loading (400–600 N). Lower fractions correspond to a smaller dentin volume subjected to critical stress levels, whereas higher fractions indicate greater dentin exposure to stresses above 60 MPa

The three stress indicators (σ_{p95}, tail gap, and $f \geq T$) provided consistent trends across materials and loading scenarios, supporting the robustness of the findings.

Total deformation analysis

Total deformation maps were generated for the highest axial (600 N) and lateral (400 N) loading conditions to illustrate the global displacement behavior of the tooth–restoration–bone complex. Under occlusal loading, deformation was primarily concentrated in the coronal portion of the restoration and gradually decreased toward the cervical region and alveolar bone (Fig. 13). In contrast, lateral loading produced higher deformation gradients, with pronounced displacement in the

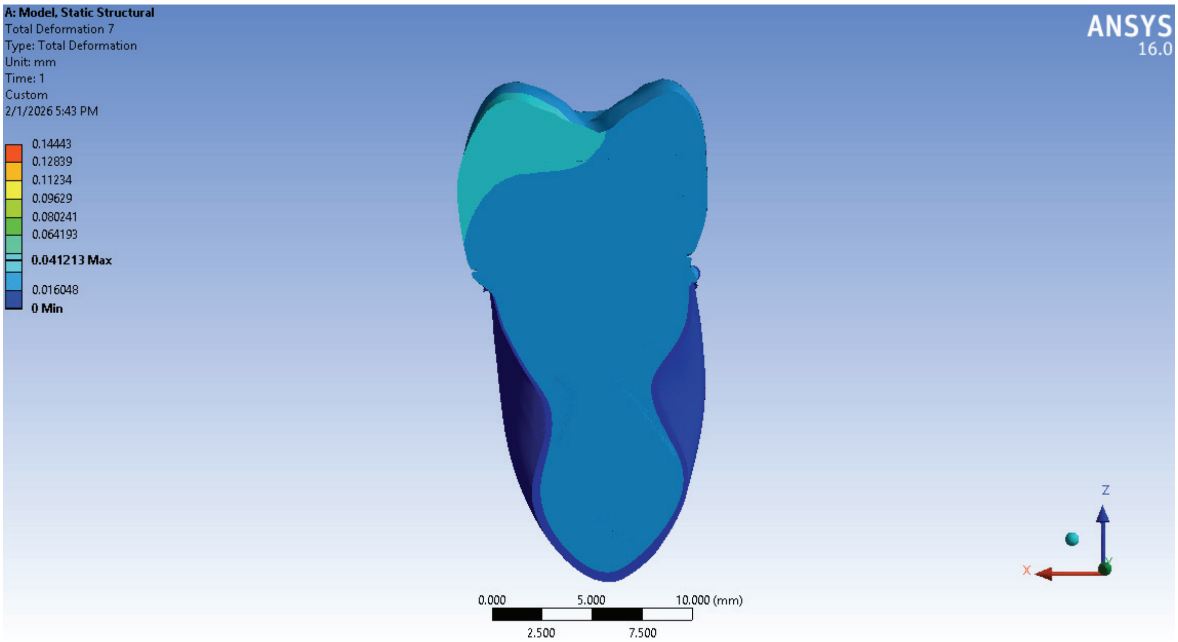

Fig. 13. Total deformation distribution of the tooth-restoration-bone complex restored with a GFR-PEEK endocrown under occlusal loading (600 N). Deformation magnitude is expressed in millimeters; deformation is magnified for visualization purposes

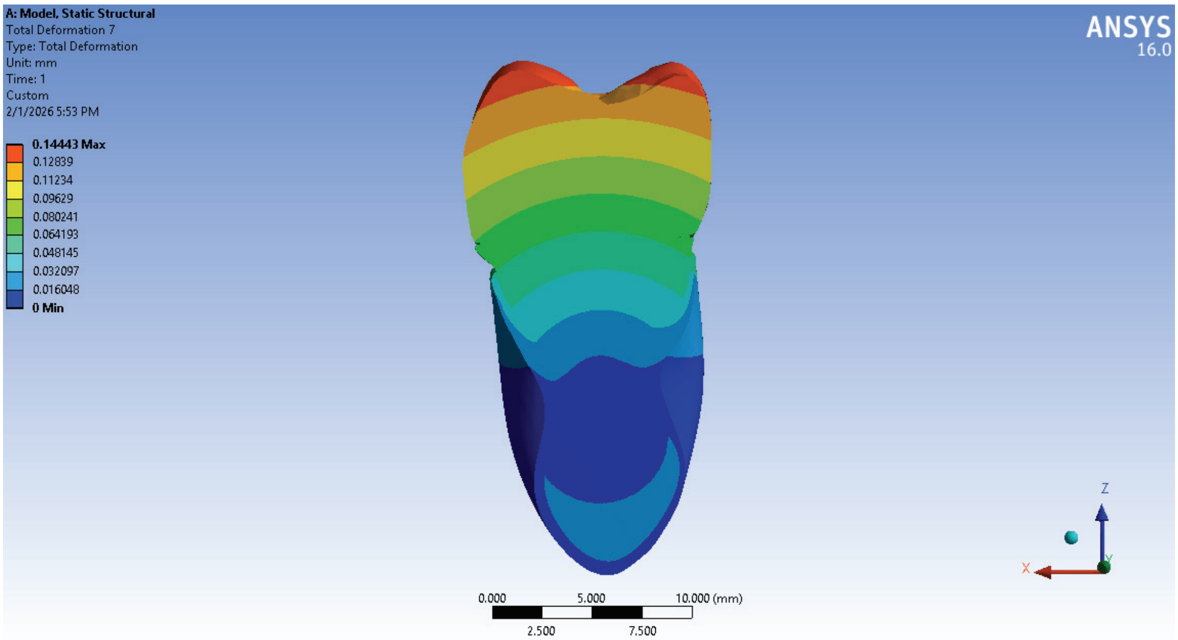

Fig. 14. Total deformation distribution of the tooth-restoration-bone complex restored with a LiDi endocrown under lateral loading (400 N). Deformation magnitude is expressed in millimeters; deformation is magnified for visualization purposes

coronal and cervical regions, associated with bending and torsional deformation patterns under non-axial loading (Fig. 14). Overall deformation of the alveolar bone remained limited under both loading conditions, consistent with the applied boundary conditions.

4. Discussion

The present study evaluated stress distribution in endodontically treated teeth restored with endocrowns under axial and lateral loading. Mechanical failure of teeth restored in this manner is commonly associated with fatigue of dental tissues resulting from cyclic masticatory loading, which highlights the importance of dentin preservation as the tissue most critically exposed to stress [12]. The results showed that all loading scenarios generated the highest stresses in dentin adjacent to the point of force application and along the crown-tooth interface. To ensure that these stress patterns reflected realistic load transfer rather than numerical artifacts, loads were applied as uniformly distributed forces over finite contact areas. This approach was adopted to avoid numerical singularities associated with point loading and to achieve a more physiologically relevant stress transfer within the tooth-restoration-bone complex. Rigid materials with a high elastic modulus, such as Co-Cr and Y-TZP, transferred loads more rigidly to the tooth, resulting in pronounced stress concentrations, particularly along preparation margins and in the cervical region [23]. In contrast, more compliant materials such as PEEK, with or without fiber reinforcement, promoted a more uniform stress distribution and lower peak values, as the restoration partially absorbed deformation [23].

The analysis of load direction further revealed that increasing the angle of force application amplified stresses within both the tooth and surrounding bone. Lateral forces had a more detrimental effect than axial forces, as they generated torsional moments and eccentric loading that concentrated stress in the cervical area. This pattern is consistent with previous studies reporting that lateral forces are critical in the initiation of cervical lesions and root microfractures [6], [16]. Such effects are particularly pronounced in maxillary premolars, which are frequently exposed to higher lateral loads; in these cases, restorative materials and designs capable of minimizing cervical and radicular stresses are especially important [37]. Consistent with prior research, lateral loading in the present study resulted in fracture initiation across all endocrown configurations, regardless of design [8].

It is well established that the fatigue threshold for human dentin ranges between 25–45 MPa [22]. Earlier studies confirmed that restorative materials with mechanical properties similar to dentin can substantially reduce the incidence of root fractures [1], [15]. In line with these findings, present study results indicate that stress tends to concentrate at the restoration-tooth interface on the loading side, confirming previous FEM observations [12].

The role of restoration volume has also been emphasized, with some studies indicating that larger volumes may compromise the mechanical resilience of the restoration itself while reducing stresses transmitted to tooth tissues [11]. Zhu et al. [39] reported that, for cement layers of ~100 μm, the buffering effect on stress transfer is negligible. Several investigations support the material--dependent stress patterns observed in present analysis. According to Zheng et al. [38], composite materials with an elastic modulus approaching that of dentin showed a more uniform stress distribution in dentin, while both high-stiffness ceramics and highly compliant polymers led to less favorable stress transfer patterns. In addition, Unsal and Yusufoglu [32] emphasized the advantages of endocrowns over post-core restorations, noting that rigid frameworks (Co-Cr) provided greater abutment protection than more flexible PEEK frameworks, which also aligns with the present results. Earlier FEM studies similarly demonstrated that materials with lower elastic modulus transmit higher stresses to residual tooth tissues, in agreement with the trends observed here [35].

An additional dimension of this problem is the role of loading regime. Lateral forces (200–400 N) generated an asymmetric stress distribution with pronounced peaks in the cervical region opposite to the point of application. In this scenario, LiDi exhibited a more favorable profile, with lower σ_{p95} and smaller tail gap values, suggesting that a homogeneous brittle ceramic – when combined with reliable adhesive bonding and ferrule support – can distribute lateral loads more diffusely through dentin without creating abrupt local concentrations. Under dominant occlusal forces of higher magnitude, GFR-PEEK effectively reduced the dentin volume exposed to stresses above critical thresholds ($f \geq 60/80/100$ MPa), which is clinically relevant for mitigating fatigue and preventing microcrack initiation.

From a clinical perspective, these findings indicate that material selection should be tailored to both tooth type and loading conditions: LiDi appears advantageous for premolars and in patients with pronounced lateral loading or parafunctional habits, owing to its more uniform stress distribution and lower risk of localized hotspots; GFR-PEEK may be preferable in molars or cases dominated by vertical loads, as reflected by its lower $f \geq T$ values and reduced dentin volume at risk of fatigue failure; while Y-TZP and Co-Cr remain suitable when maximum rigidity and strength are required, but should be used cautiously and primarily when adequate ferrule and wall height are available. It must also be acknowledged that all restorative materials were modeled as homogeneous and isotropic, which does not fully reflect their true structural complexity, and that the exclusion of cement properties represents a significant limitation, as the cement layer may influence load transfer and stress attenuation. In addition, the numerical model was based on a single representative mandibular molar geometry, and potential variations in tooth anatomy were not explicitly addressed. Within these limitations, the present findings confirm that restorative material selection has a decisive influence on how functional loads are distributed within dentin, with Co-Cr and Y-TZP associated with more rigid load transfer and localized peaks, PEEK-based systems demonstrating stress absorption and lower critical volumes, and LiDi occupying an intermediate position with a favorable response to lateral loading. These outcomes underline the clinical importance of material selection according to tooth type and loading pattern in order to optimize the biomechanical performance and longevity of endocrowns.

Restoration failure is strongly influenced by local stress concentrations and damage accumulation under cyclic masticatory loads [25]. Accordingly, the present FEM simulations are intended to provide a comparative assessment of stress patterns within the restored tooth rather than a direct prediction of fatigue life. A more physiological representation (e.g., explicit periodontal ligament and bone compliance) could affect absolute displacement levels, however, because bone stresses/displacements were outside the scope of this work, the simplified support was considered adequate for the intended within-tooth evaluation [25], [27].

5. Conclusions

The present study supports the concept that no single material is universally optimal. For teeth predominantly subjected to lateral loading, LiDi demonstrated a more favorable and uniform stress profile (lower σ_{p95} and tail gap), whereas under higher axial forces GFR-PEEK effectively reduced the dentin volume exposed to critical stress levels (lower $f \geq T$). In both scenarios, a well-designed ferrule and reliable adhesion remain essential for biomechanical stability and long-term success of endocrowns.

Considering the well-known limitations of the finite element method (FEM), future studies may benefit from supplementing purely numerical assessments with targeted experimental work. In particular, incorporating fatigue testing and similar validation approaches could help verify the analytical predictions and increase confidence in the proposed models.

Ethical statements

Prior to use, the patient provided written informed consent for the research use of the tooth specimen. In accordance with the Declaration of Helsinki and institutional guidelines, studies conducted exclusively on anonymized extracted teeth do not require additional ethical clearance.

Acknowledgements

The part of this research is funded by Ministry of Science, Technological Development and Innovation of the Republic of Serbia, Contract No. 451-03-65/2024-03/200155.

References

[1] ASMUSSEN E., PEUTZFELDT A., HEITMANN T., *Stiffness, elastic limit, and strength of newer types of endodontic posts*, J. Dent., 1999, 27 (4), 275–278, DOI: 10.1016/S0300-5712(98)00066-9.

[2] AVERSA R., APICELLA D., PERILLO L., SORRENTINO R. et al., *Non-linear elastic three-dimensional finite element analysis on the effect of endocrown material rigidity on alveolar bone remodeling process*, Dent. Mater., 2009, 25 (5), 678–690, DOI: 10.1016/j.dental.2008.10.015.

[3] BATISTA A., PALACIOS N., ALVARADO JIMÉNEZ O.R., *Zirconia cementation: a systematic review of the most currently used protocols*, Open Dent. J., 2024, 18, e18742106300869, DOI: 10.2174/0118742106300869240621074459.

[4] CHANG Y.H., LIN W.H., KUO W.C., CHANG C.Y., LIN C.L., *Mechanical interactions of cuspal-coverage designs and cement thickness in a cusp-replacing ceramic premolar restoration: a finite element study*, Med. Biol. Eng. Comput., 2009, 47 (4), 367–374, DOI: 10.1007/s11517-008-0379-y.

[5] CHEN X., MAO B., ZHU Z., YU J. et al., *A three-dimensional finite element analysis of mechanical function for 4 removable partial denture designs with 3 framework materials: CoCr, Ti-6Al-4V alloy and PEEK*, Sci. Rep., 2019, 9, 13975, DOI: 10.1038/s41598-019-50363-1.

[6] DJEBBAR N., SERIER B., BOUIADJRA B.B., BENBAREK S. et al., *Analysis of the effect of load direction on the stress distribution in dental implant*, Mater. Des., 2010, 31 (4), 2097–2101, DOI: 10.1016/j.matdes.2009.10.042.

[7] DO T.T., TRINH T.M., TRAN T.T.P., NGUYEN V.T.T., LE L.N., *Clinical performance of computer-aided design/computer-aided manufacture lithium disilicate ceramic endocrown restorations: A 2-year study*, J. Conserv. Dent. Endod., 2024, 27 (1), 51–56, DOI: 10.4103/JCDE.JCDE_99_23.

[8] EL GHOUL W.E., ÖZCAN M., TRIBST J.P.M., SALAMEH Z., *Fracture resistance, failure mode and stress concentration in a modified endocrown design*, Biomater. Investig. Dent., 2020, 7 (1), 110–119, DOI: 10.1080/26415275.2020.1801348.

[9] ELSAID S.T., AHMED A., HASSAN S.M., *Fracture resistance and retention of CAD/CAM endo-crowns using different preparation designs*, Al-Azhar Dent. J., 2020, 7 (2), Article 17, DOI: 10.21608/adjg.2020.13052.1147.

[10] GOVARE N., CONTREPOIS M., *Endocrowns: a systematic review*, J. Prosthet. Dent., 2020, 123 (3), 411–418.e9, DOI: 10.1016/j.prosdent.2019.04.009.

[11] GULEC L., ULUSOY N., *Effect of endocrown restorations with different CAD/CAM materials: 3D finite element and Weibull analyses*, Biomed. Res. Int., 2017, 2017, 5638683, DOI: 10.1155/2017/5638683.

[12] HASAN I., FRENTZEN M., UTZ K.H., HOYER D., LANGENBACH A., BOURAUEL C., *Finite element analysis of adhesive endo-crowns of molars at different height levels of buccally applied load*,

J. Dent. Biomech., 2012, 3, 1758736012455421, DOI: 10.1177/1758736012455421.

[13] HUANG T.J., SCHILDER H., NATHANSON D., *Effects of moisture content and endodontic treatment on some mechanical properties of human dentin*, J. Endod., 1992, 18 (5), 209–215, DOI: 10.1016/S0099-2399(06)81262-8.

[14] ISHAK M.I., DAUD R., MOHD NOOR S.N.F., KHOR C.Y., ROSLAN H., *Assessment of stress shielding around a dental implant for variation of implant stiffness and parafunctional loading using finite element analysis*, Acta Bioeng. Biomech, 2022, 24 (3), 147–159, DOI: 10.37190/ABB-02129-2022-02.

[15] ISIDOR F., ODMAN P., BRØNDUM K., *Intermittent loading of teeth restored using prefabricated carbon fiber posts*, Int. J. Prosthodont., 1996, 9 (2), 131–136.

[16] KAMENSKIKH A.A., SAKHABUTDINOVA L., ASTASHINA N., PETRACHEV A. et al., *Numerical modeling of a new type of prosthetic restoration for non-carious cervical lesions*, Materials, 2022, 15 (15), 5102, DOI: 10.3390/ma15155102.

[17] LIN C.L., CHANG Y.H., CHANG C.Y., PAI C.A. et al., *Finite element and Weibull analyses to estimate failure risks in the ceramic endocrown and classical crown for endodontically treated maxillary premolar*, Eur. J. Oral Sci., 2010, 118 (1), 87–93, DOI: 10.1111/j.1600-0722.2009.00704.x.

[18] MACERI F., MARTIGNONI M., VAIRO G., *Mechanical behaviour of endodontic restorations with multiple prefabricated posts: a finite-element approach*, J. Biomech., 2007, 40 (11), 2386–2398, DOI: 10.1016/j.jbiomech.2006.11.018.

[19] MONTEIRO J.B., DAL PIVA A.M.O., TRIBST J.P.M., BORGES A.L.S., TANGO R.N., *The effect of resection angle on stress distribution after root-end surgery*, Iran Endod J., 2018, 13 (2), 188–194, DOI: 10.22037/iej.v13i2.19089.

[20] MÖRMANN W.H., BINDL A., LÜTHY H., RATHKE A., *Effects of preparation and luting system on all-ceramic computer-generated crowns*, Int. J. Prosthodont., 1998, 11 (4), 333–339.

[21] NAHAR R., MISHRA S.K., CHOWDHARY R., *Evaluation of stress distribution in an endodontically treated tooth restored with four different post systems and two different crowns: a finite element analysis*, J. Oral Biol. Craniofac. Res., 2020, 10 (4), 719–726, DOI: 10.1016/j.jobcr.2020.10.004.

[22] NALLA R.K., KINNEY J.H., MARSHALL S.J., RITCHIE R.O., *On the in vitro fatigue behavior of human dentin: effect of mean stress*, J. Dent. Res., 2004, 83 (3), 211–215, DOI: 10.1177/154405910408300305.

[23] OYAR P., ULUSOY M., ESKITAŞÇIOĞLU G., *Finite element analysis of stress distribution in ceramic crowns fabricated with different tooth preparation designs*, J. Prosthet. Dent., 2014, 112 (4), 871–877, DOI: 10.1016/j.prosdent.2013.12.019.

[24] PAPALEXOPOULOS D., SAMARTZI T.-K., SARAFIANOU A., *A thorough analysis of the endocrown restoration: a literature review*, J. Contemp. Dent. Pract., 2021, 22 (4), 422–426, DOI: 10.5005/jp-journals-10024-3075.ECA.

[25] PIENIAK D., NIEWCZAS A.M., *Phenomenological evaluation of fatigue cracking of dental restorations under conditions of cyclic mechanical loads*, Acta Bioeng. Biomech., 2012, 14 (2), 10–18, DOI: 10.5277/abb120202.

[26] QIN L., YAO S., ZHAO J., ZHOU C. et al., *Review on development and dental applications of polyetheretherketone-based biomaterials and restorations*, Materials, 2021, 14 (2), 408, DOI: 10.3390/ma14020408.

[27] SARCEV I.N., PETRONIJEVIC B.S., ATANACKOVIC T.M., *A biomechanical model for a new incremental technique for tooth restoration*, Acta Bioeng. Biomech., 2012, 14 (3), 86–92, DOI: 10.5277/abb120312.

[28] SCHWITALLA A.D., ABOU-EMARA M., SPINTIG T., LACKMANN J. et al., *Finite element analysis of the biomechanical effects of PEEK dental implants on the peri-implant bone*, J. Biomech., 2015, 48 (1), 1–7, DOI: 10.1016/j.jbiomech.2014.11.017.

[29] SHAMS A., ELSHERBINI M., ELSHERBINY A.A., ÖZCAN M., SAKRANA A.A., *Rehabilitation of severely destructed endodontically treated premolar teeth with novel endocrown system: biomechanical behavior assessment through 3D finite element and in vitro analyses*, J. Mech. Behav. Biomed. Mater., 2022, 126, 105031, DOI: 10.1016/j.jmbbm.2021.105031.

[30] SIOUSTIS I.-A., AXINTE M., PRELIPCEANU M., MARTU A., KAPPENBERG-NITESCU D.-C., TESLARU S., LUCHIAN I., SOLOMON S.M., CIMPOESU N., MARTU S., *Finite element analysis of mandibular anterior teeth with healthy, but reduced periodontium*, Appl. Sci., 2021, 11 (9), 3824, DOI: 10.3390/app11093824.

[31] TOPARLI M., GÖKAY N., AKSOY T., *Analysis of a restored maxillary second premolar tooth by using three-dimensional finite element method*, J. Oral Rehabil., 1999, 26 (2), 157–164, DOI: 10.1046/j.1365-2842.1999.00342.x.

[32] UNSAL G.S., YUSUFOGLU S.I., *Finite element analysis of endocrown and post-and-core abutments for removable partial dentures with different framework materials*, Int. J. Prosthodont., 2023, 36 (2), 203–215, DOI: 10.11607/ijp.7269.

[33] URICIUC W.A., BOŞCA A.B., BĂBŢAN A.M., VERMEŞAN H. et al., *Study on the surface of cobalt-chromium dental alloys and their behavior in oral cavity as cast materials*, Materials, 2022, 15 (9), 3052, DOI: 10.3390/ma15093052.

[34] WALCZAK K., RUES S., WIECKIEWICZ M., RANGE U., SCHMITTER M., *Is mechanical retention for adhesive core build-up needed to restore a vital tooth with a monolithic zirconium crown? – An in vitro study*, Acta Bioeng. Biomech., 2016, 18 (4), 118–126, DOI: 10.5277/ABB-00529-2015-02.

[35] YAMANEL K., CAĞLAR A., GÜLSAHI K., ÖZDEN U.A., *Effects of different ceramic and composite materials on stress distribution in inlay and onlay cavities: three-dimensional finite element analysis*, Dent. Mater. J., 2009, 28 (6), 661–670, DOI: 10.4012/dmj.28.661.

[36] ZARONE F., SORRENTINO R., APICELLA D., VALENTINO B. et al., *Evaluation of the biomechanical behavior of maxillary central incisors restored by means of endocrowns compared to a natural tooth: a 3D static linear finite elements analysis*, Dent. Mater., 2006, 22 (11), 1035–1044, DOI: 10.1016/j.dental.2005.11.034.

[37] ZHANG Y., LAI H., MENG Q., GONG Q. et al., *The synergetic effect of pulp chamber extension depth and occlusal thickness on stress distribution of molar endocrowns: a three-dimensional finite element analysis*, J. Mater. Sci. Mater. Med., 2022, 33, 56, DOI: 10.1007/s10856-022-06677-0.

[38] ZHENG Z., SUN J., JIANG L., WU Y. et al., *Influence of margin design and restorative material on the stress distribution of endocrowns: a 3D finite element analysis*, BMC Oral Health, 2022, 22 (1), 30, DOI: 10.1186/s12903-022-02063-y.

[39] ZHU J., WANG D., RONG Q., QIAN J. et al., *Effect of central retainer shape and abduction angle during preparation of teeth on dentin and cement layer stress distributions in endocrown-restored mandibular molars*, Dent. Mater. J., 2020, 39 (3), 464–470, DOI: 10.4012/dmj.2019-050.